Available online at www.sciencedirect.com
ScienceDirect
Control Engineering Practice 16 (2008) 991–1003
CONTROL ENGINEERING PRACTICE
www.elsevier.com/locate/conengprac

Robust control of piecewise linear systems: A case study in sheet flow control ☆

J.J.T.H. de Best*, B.H.M. Bukkems, M.J.G. van de Molengraft, W.P.M.H. Heemels, M. Steinbuch

Dynamics and Control Technology Group, Department of Mechanical Engineering, Technische Universiteit Eindhoven, P.O. Box 513, 5600 MB Eindhoven, The Netherlands

Received 1 November 2006; accepted 10 October 2007
Available online 28 November 2007

Abstract

This paper presents a control design approach for robust sheet control in a printer paper path. By splitting up the control problem into low level motor control loops and a high level sheet control loop, a hierarchical control structure is obtained. Based on the piecewise linear model of the high level sheet dynamics, the control design is formulated in the H_∞ framework. The resulting dynamic output feedback controllers guarantee stability and performance of the closed-loop system. To show the effectiveness of the control design approach in practice, the robust sheet controllers are successfully implemented on an experimental paper path setup.

Keywords: Piecewise linear systems; Hierarchical control; Robust control; Linear matrix inequalities

1. Introduction

High productivity and good printing accuracy are two of the main requirements for high volume cut sheet document handling systems. One of the dominating factors in satisfying these requirements is the reliable transportation of the sheets through the paper path. An example of such a paper path is shown in Fig. 1. Sheets enter the paper path at the paper input module, here referred to as PIM. After the sheets have been transported through the preheater units to obtain the desired temperature required for printing, the sheets go to the image transfer station (ITS) where they meet their corresponding images. For the purpose of backside printing, sheets can re-enter the paper path via the so-called duplex loop. Eventually, sheets are transported to the finisher (FIN) where they are collected. The transportation of the sheets is realized via so-called pinches. These pinches consist of a driven roller and a non-driven roller. The task of the non-driven roller is to apply sufficient normal force in order to prevent the sheet from slipping in the pinch. As can be seen from Fig. 1, these pinches can either be driven by one motor individually or they can be grouped into sections.

In order to achieve a good printing quality, the sheet transportation system must deliver the sheets on time at the ITS and maintain the right sheet velocity in order to prevent misplaced or blurred images. In today's cut sheet printers the transportation of the sheets mainly relies on event-driven closed-loop sheet control in combination with time-driven closed-loop motor control. Together with a high precision mechanical design with small manufacturing tolerances, this ultimately results in a predictable sheet flow. At discrete points in the paper path, i.e. where the optical sheet sensors are located, the presence of a sheet is detected. Based on this information, the reference velocities of the motor can be adjusted in order to correct for possible errors. A drawback of this event-driven closed-loop sheet

☆ This work has been carried out as part of the Boderc project under the responsibility of the Embedded Systems Institute. This project is partially supported by the Netherlands Ministry of Economic Affairs under the Senter TS program.

*Corresponding author. Tel.: +31 40 247 4227; fax: +31 40 246 1418.
E-mail addresses: J.J.T.H.d.Best@tue.nl (J.J.T.H. de Best), bjorn.bukkems@tmc.nl (B.H.M. Bukkems), M.J.G.v.d.Molengraft@tue.nl (M.J.G. van de Molengraft), W.P.M.H.Heemels@tue.nl (W.P.M.H. Heemels), M.Steinbuch@tue.nl (M. Steinbuch).

0967-0661/$ - see front matter © 2007 Elsevier Ltd. All rights reserved.
doi:10.1016/j.conengprac.2007.10.004

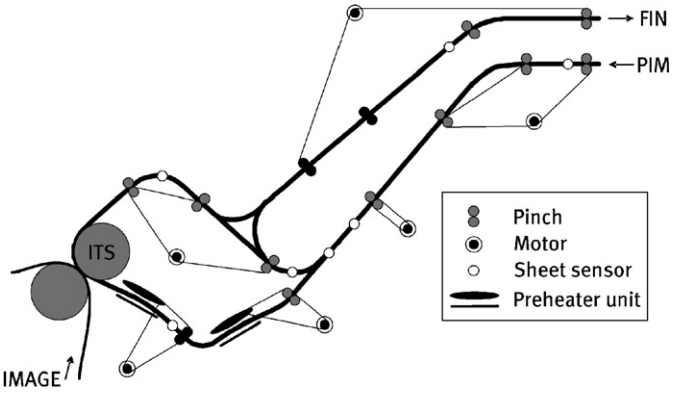

Fig. 1. Example of an industrial printer paper path.

control approach is the limited robustness against uncertainties and disturbances. Furthermore, high precision mechanics are needed to obtain the desired predictability in the sheet flow, which leads to a relatively high cost of goods. An alternative for tackling the sheet feedback control problem is to exploit the power of closed-loop sheet feedback control (Bukkems, de Best, van de Molengraft, & Steinbuch, 2006; Bukkems, 2007; Cloet, 2001; Kruciński, 2000; Rai, 1998). In the closed-loop approach, the tolerances in the mechanical design are allowed to be larger, since in this case active sheet feedback control is used to react on disturbances and uncertainties present in the printer paper path. To implement sheet feedback control, it is necessary to have knowledge of the sheet position. This can, for example, be realized by adding (cheap) position sensors, possibly in combination with model-based observer techniques.

The design of closed-loop sheet feedback control is mostly based on dynamic paper path models. In Cloet (2001) and Kruciński (2000), the dynamics are split up into low level section dynamics and high level sheet dynamics. The section dynamics map the motor currents to the angular velocities, implying that these dynamics are basically described by integrators. The high level sheet dynamics map the section velocities to the sheet position, which is described by a switching integrator. The combination of the finite state machine describing the sheet dynamics and the integrators describing the section dynamics leads to a hybrid dynamic model, and the control problem is formulated in a hybrid hierarchical control setup, in which the spacing between the sheets is controlled. However, in Kruciński (2000) and Cloet (2001) the control design is based on intuition and verified only by simulation. Stability of the closed-loop system is not proven and disturbances and uncertainties present in the printer paper path are not taken into account in the proposed control design.

In this paper a model-based feedback control design procedure is proposed that does guarantee stability and performance of the closed-loop system subject to disturbances and uncertainties. As in Cloet (2001) and Kruciński (2000) the control problem is split up into two levels, namely in low level motor control loops and a high level sheet control loop. For the control design of the high level sheet controller the low level motor control loops are assumed to be ideal. As a result, the high level sheet dynamics are described by switching integrators, which will be formulated in the piecewise linear (PWL) modeling formalism (Heemels, Schutter, & Bemporad, 2001; Sontag, 1981). As such, the control problem at hand is transformed into a tracking control problem for PWL systems. An H_∞, or more precise, an $\mathscr{L}_2$ gain approach will be adopted to tackle this problem. Known results from literature regarding H_∞ control of piecewise affine systems can be found in Rantzer and Johansson (2000) and Feng (2002a), in which *state* feedback controllers are used. Extensions for controlling *uncertain* PWL systems via state feedback are presented in Feng (2002b) and Chen, Zhu, and Feng (2004). In this paper, extensions of these existing works will be presented and apply these within the sheet feedback control application. The first contribution is a controller synthesis technique that is based on *output* feedback as opposed to the results in Feng (2002b), Chen et al. (2004), Rantzer and Johansson (2000) and Feng (2002a), that all are based on state feedback. In particular, for carrying out the controller synthesis, LMI-based approaches for linear systems known in literature, e.g. Gahinet and Apkarian (1994), Gahinet (1996) and Scherer, Gahinet, and Chilali (1997), are extended to the PWL case. Secondly, frequency domain weighting filters will be used (as commonly used in the linear case) to shape the closed-loop dynamics of the PWL sheet flow model. The novelty here lies in the fact that this is the first paper in which the classical linear H_∞ loop shaping techniques (Skogestad & Postlethwaite, 2005) using weighting filters is combined with stability and performance requirements for the overall PWL system. Allowing for frequency dependent weighing of the performance variables, defined in the sheet feedback control problem as the weighted sheet tracking error or the weighted sheet position, in combination with the weighted controller output, is important because performance can now be enforced where it is needed most. Moreover, with the use of weighting filters, an ability is created to include additional dynamics in the controller, like for example a high frequency roll-off for the individual subsystems. The third contribution of this paper is the practical demonstration of the control design theory. Experiments will confirm the robustness for parametric model uncertainties of the closed-loop PWL system. It will be shown that the desired tracking performance is realized using the presented control design approach.

The remainder of this paper is organized as follows: in Section 2, the system under consideration will be discussed in more detail and the problem statement will be given, together with the control goal. In Section 3, the nominal control design approach (without uncertainties) is discussed, whereas in Section 4 the control design is presented in case the uncertainties are included. In Section 5, the experimental setup, that is used to validate the proposed control design will be discussed. The results of these experiments are given in Section 6, which at the end are followed by the conclusions and recommendations.

2. Sheet feedback control problem

Although the paper path depicted in Fig. 1 has many challenging aspects, such as for example the coupled pinches and the duplex loop, a more basic paper path is considered. By considering this basic paper path, shown in Fig. 2, insight in the essence of the control problem, which lies in the consecutive switching of the driving pinch, is obtained. The paper path under consideration consists of three pinches, located at x_{p1}, x_{p2}, and x_{p3}, which are all driven by separate motors. The distance between the three pinches is chosen equal to the sheet length L_s, so sheets cannot be in more than one pinch at the same time. The transmission ratios between motor and pinch are denoted by n_i and the radii of the driven pinches are denoted by R_i, $i \in \mathscr{I}$, with $\mathscr{I} = \{1, 2, 3\}$ the index set of the sheet regions. No slip is assumed to be present between the sheet and the pinches and the gear belt between the motor and pinches is assumed to be infinitely stiff. The mass of the sheet is assumed to be zero and the sheet position $x_s(t)$ is assumed to be known at all times t. These assumptions are further discussed in Bukkems (2007). The control problem is formulated in a hierarchical control architecture, which is not new in itself and can be found in the different application domains (Cloet, 2001; Kruciński, 2000; Tang, Landers, & Balakrishnan, 2006; Yasar & Ray, 2007). We seek to apply such a control approach within a printer paper path. It consist of low level motor control loops and a high level sheet control loop. The task of the low level motor control loops is to track a reference velocity, which is prescribed by the high level sheet controller, and to account for disturbances and uncertainties present at the motor level, such as, for example, friction in bearings. The task of the high level sheet control loop is to track the sheet position reference profile and to account for disturbances and uncertainties present at the sheet level. One can think of, for example, tolerances on the pinch radii or varying sheet characteristics related to geometry or roughness. In this way, the overall complex control problem is reformulated into two simpler control problems. This involves in the first place the design of low level single-input single-output (SISO) motor control loops and, secondly, the design of a high level sheet control loop where the motor control loops and sheet control loop are closed sequentially. The resulting hierarchical control structure requires

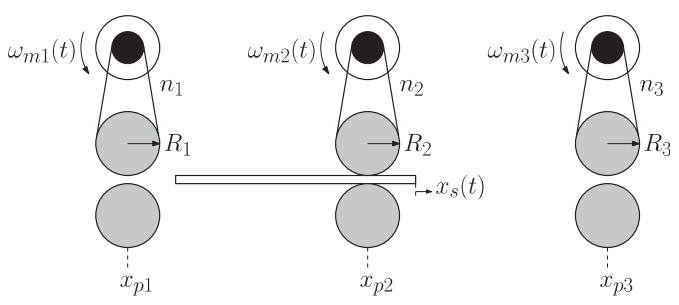

Fig. 2. Basic printer paper path.

the inner loops to have a higher bandwidth, here defined as equivalent to the cross-over frequency, than the outer loop (Stephanopoulos, 1984). Moreover, the inner loops should be designed such that the reference velocity profiles generated by the outer loop will be closely tracked. The control goal that is adopted for the basic paper path case study is, given the low level closed-loop motor dynamics and a model of the high level sheet dynamics, the design of high level sheet feedback controllers (HLCs) that yield a stable and robust closed-loop system and track the desired sheet reference profiles such that the performance specifications are satisfied. More specifically, the sheet motion task is defined as to track reference position signals $x_{s,r}$ (that typically will be linear position profiles (ramps) corresponding to constant reference velocities $\dot{x}_{s,r}$) with robust stability and robust performance in the presence of parametric uncertainties in the transmission ratios n_i and the pinch radii R_i, $i = 1, 2, 3$. The performance requirements for the problem are defined as the vanishing of the *transient* tracking error before entering the next section and upper bounding the *steady state* errors by 5×10^{-4} m.

The inner loops of the hierarchical control structure, i.e. the low level motor control loops, are designed using well-known SISO loop shaping techniques for linear time-invariant systems (Franklin, Powell, & Emami-Naeini, 1994). In the Laplace domain, the closed-loop motor dynamics can be represented as

$$\Omega_{mi}(s) = T_{mi}(s)\Omega_{mi,r}(s), \quad i \in \mathscr{I}, \tag{1}$$

with $T_{mi}(s)$ the complementary sensitivity of the closed-loop motor dynamics i, which maps the motor reference velocities $\omega_{mi,r}(t)$ to the actual motor velocities $\omega_{mi}(t)$. In (1), the Laplace transforms of $\omega_{mi}(t)$ and $\omega_{mi,r}(t)$ are denoted by $\Omega_{mi}(s)$ and $\Omega_{mi,r}(s)$, respectively, with $s \in \mathbb{C}$. In the control design of the HLCs it is assumed that the low level motor control loops are ideal, i.e. $T_{mi}(s) = 1$, $\forall i \in \mathscr{I}$. In practice, however, the bandwidth of the low level control loops can be relaxed, while preserving the requirement that the low level bandwidths should be significantly higher than the bandwidth of the high level control loop. Because of this simplifying assumption in the control design, an a posteriori stability check, mentioned in Section 6.1, can be carried out before implementing the high level sheet feedback controllers in practice.

In the outer loop of the hierarchical control structure, i.e. the high level sheet control loop, modeling and control of the sheet dynamics are considered. Due to the assumption of ideal low level motor control loops, the motor velocities, as calculated by the high level sheet controllers, are the actual velocity input $\omega_{mi}(t)$ to the high level sheet dynamics. This is shown in Fig. 3, which represents the high level control scheme. Due to the fact that the stiffness between the motor and pinch is assumed to be infinitely large and no slip is assumed between the sheet and pinch, the sheet velocity can be directly calculated from the motor velocities via straightforward holonomic kinematic constraint relations. Since at each

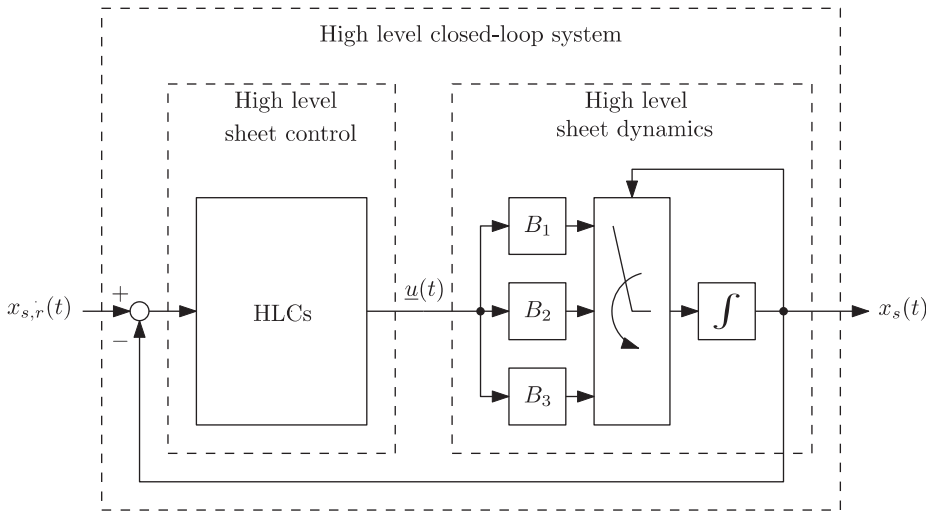

Fig. 3. High level control scheme.

time instant the sheet can only be in one pinch, the input of the sheet dynamics will change when the sheet enters the next pinch. This consecutive switching of the driving pinch is captured in the PWL modeling formalism (Sontag, 1981). The high level sheet dynamics are therefore given by

$$\dot{x}_s(t) = B_i\,\underline{u}(t), \quad x_s(t) \in \mathscr{X}_i,\ i \in \mathscr{I}, \tag{2}$$

where $x_s(t)$ is the sheet position, i.e. the position of the leading of the sheet, at time t and the input matrices B_i are defined as $B_1 = [n_1R_1\ 0\ 0]$, $B_2 = [0\ n_2R_2\ 0]$ and $B_3 = [0\ 0\ n_3R_3]$. The nominal transmission ratios are chosen to be $n_1 = \frac{18}{37}$, $n_2 = \frac{14}{30}$, and $n_3 = \frac{15}{30}$, whereas the nominal radii R_i of the driven rollers are all equal to 14×10^{-3} m. The input vector is defined as $\underline{u}(t) = [\omega_{m1}(t)\ \omega_{m2}(t)\ \omega_{m3}(t)]^{\mathrm{T}}$. Furthermore, the partitioning of the sheet regions is given by $\{\mathscr{X}_i\}_{i\in\mathscr{I}} \subset \mathbb{R}$. Here, $\mathscr{X}_1 = \{x_s(t)|x_s(t) \in [x_{p1}, x_{p2})\}$, $\mathscr{X}_2 = \{x_s(t)|x_s(t) \in [x_{p2}, x_{p3})\}$ and $\mathscr{X}_3 = \{x_s(t)|x_s(t) \in [x_{p3}, x_{p3} + L_s)\}$, with $x_{p1} < x_{p2} < x_{p3}$.

3. Nominal control design

3.1. Controller synthesis

This section describes the design of high level H_∞ sheet feedback controllers based on the model of the high level sheet dynamics (2) assuming both the absence of uncertainties in the system parameters and the absence of disturbances acting on the system. In the approach presented, linear H_∞ loop shaping techniques for each subsystem (Skogestad & Postlethwaite, 2005) are combined with stability and performance requirements for the PWL system. Regarding the control design for each subsystem, it is desirable that the high level sheet feedback controllers in these subsystems have integral action, which results in a high gain at low frequencies, in order to accurately track the sheet reference trajectory. Furthermore, it is desired to enforce the high level sheet controllers to have a roll-off at high frequencies in order to prevent the low level motor

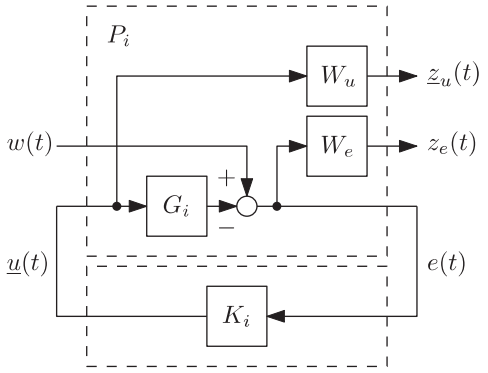

Fig. 4. Augmented high level control scheme.

control loops to be excited by high frequencies which cannot be tracked, as in reality the low level motor control loops are not ideal, i.e. not satisfying $T_{mi}(s) = 1$ in (1). Both the integral action and the high frequency roll-off can be incorporated in the high level sheet controllers by constructing an augmented plant, that besides the nominal high level sheet dynamics contains weighting filters for shaping the closed-loop transfer functions. The augmented plant P_i for region i is schematically depicted in Fig. 4. The sheet reference trajectory $x_{s,r}(t)$ is taken as the exogenous input $w(t)$ of the augmented plant. The outputs to be minimized are the weighted sheet tracking error $z_e(t)$ and the weighted high level sheet controller output $\underline{z}_u(t)$. The measured output is the sheet tracking error $e(t)$. The output of the high level controllers, i.e. the column with motor reference velocities, is equal to $\underline{u}(t)$ as in (2). As can be seen from Fig. 4 the weighting filter W_e is used to shape the sensitivity

$$S_i = (I + G_iK_i)^{-1}, \quad i \in \mathscr{I}, \tag{3}$$

where $G_i(s) = (1/s)B_i$ represents the high level sheet dynamics in region i and K_i denotes the high level sheet controller in region i. Given the filter W_e the desired bandwidth of the sheet control loop and the integral action can be enforced. The SISO filter W_e is given by the

state-space realization

$$\begin{aligned}\dot{\underline{x}}_{W_e}(t) &= A_{W_e}\underline{x}_{W_e}(t) + B_{W_e}e(t),\\ z_e(t) &= C_{W_e}\underline{x}_{W_e}(t) + D_{W_e}e(t),\end{aligned} \tag{4}$$

where $\underline{x}_{W_e}$ represents the state vector of the filter. The second filter, W_u, is used to shape the control sensitivity function, defined by

$$R_i = (I + K_iG_i)^{-1}K_i, \quad i \in \mathscr{I}. \tag{5}$$

This filter is used to enforce a high frequency roll-off in the high level sheet controllers for each regime. The multi-input multi-output (MIMO) filter W_u is given as follows:

$$\begin{aligned}\dot{\underline{x}}_{W_u}(t) &= A_{W_u}\underline{x}_{W_u}(t) + B_{W_u}\underline{u}(t),\\ \underline{z}_u(t) &= C_{W_u}\underline{x}_{W_u}(t) + D_{W_u}\underline{u}(t)\end{aligned} \tag{6}$$

with $\underline{x}_{W_u}$ representing the state vector of the filter. Given the weighting filters W_e and W_u, together with the high level sheet dynamics (2), and by defining $\underline{z} = [z_e\ \underline{z}_u^{\mathrm{T}}]^{\mathrm{T}}$, $\underline{x} = [x_s\ \underline{x}_{W_e}^{\mathrm{T}}\ \underline{x}_{W_u}^{\mathrm{T}}]^{\mathrm{T}}$ the augmented plant can be represented as (Scherer et al., 1997)

$$\begin{aligned}\dot{\underline{x}}(t) &= A_i\,\underline{x}(t) + B_{w,i}w(t) + B_{u,i}\,\underline{u}(t)\\ \underline{z}(t) &= C_{z,i}\,\underline{x}(t) + D_{zw,i}w(t) + D_{zu,i}\,\underline{u}(t). \quad x_s(t) \in \mathscr{X}_i,\ \ i \in \mathscr{I}.\\ e(t) &= C\,\underline{x}(t) + D_{w,i}w(t)\end{aligned} \tag{7}$$

As a natural structure for the high level sheet controller, the following is proposed:

$$\begin{aligned}\dot{\underline{\xi}}(t) &= A_{K,i}\,\underline{\xi}(t) + B_{K,i}e(t),\\ \underline{u}(t) &= C_K\,\underline{\xi}(t) + D_Ke(t)\end{aligned} \qquad x_s(t) \in \mathscr{X}_i,\ \ i \in \mathscr{I}, \tag{8}$$

with $\underline{\xi}$ the (shared) controller state. The choice for constant matrices C_K and D_K can be explained by the fact that in this case it is ensured that there are no jumps in the controller outputs, i.e. the reference velocities for the low level motor control loops. Substitution of (8) into (7) yields the closed-loop dynamics

$$\begin{aligned}\dot{\underline{x}}_{CL}(t) &= \mathscr{A}_i\underline{x}_{CL}(t) + \mathscr{B}_iw(t),\\ \underline{z}(t) &= \mathscr{C}_i\underline{x}_{CL}(t) + \mathscr{D}_iw(t)\end{aligned} \qquad x_s(t) \in \mathscr{X}_i,\ \ i \in \mathscr{I}, \tag{9}$$

with

$$\left(\begin{array}{c|c}\mathscr{A}_i & \mathscr{B}_i\\ \hline \mathscr{C}_i & \mathscr{D}_i\end{array}\right) = \left(\begin{array}{cc|c} A_i + B_{u,i}D_KC & B_{u,i}C_K & B_{w,i} + B_{u,i}D_KD_{w,i}\\ B_{K,i}C & A_{K,i} & B_{K,i}D_{w,i}\\ \hline C_{z,i} + D_{zu,i}D_KC & D_{zu,i}C_K & D_{zw,i} + D_{zu,i}D_KD_{w,i}\end{array}\right),\ \ i \in \mathscr{I} \tag{10}$$

and $\underline{x}_{CL} = [\underline{x}^{\mathrm{T}}\ \underline{\xi}^{\mathrm{T}}]^{\mathrm{T}}$ the closed-loop state vector. If the closed-loop PWL system (9) admits a *common* quadratic Lyapunov function[1]

$$V(\underline{x}_{CL}) = \underline{x}_{CL}^{\mathrm{T}}\mathscr{P}\underline{x}_{CL}, \tag{11}$$

with $\mathscr{P}$ a positive definite matrix such that

$$\mathscr{A}_i^{\mathrm{T}}\mathscr{P} + \mathscr{P}\mathscr{A}_i < 0, \quad i \in \mathscr{I}, \tag{12}$$

then the controllers for each individual subsystem are stabilizing (Scherer et al., 1997; Zhou, Doyle, & Glover, 1996) and the closed-loop PWL system is globally asymptotically stable (GAS) (for zero external variables w).

Using the dissipativity reasoning similarly as in the linear case (cf. Gahinet, 1996; Gahinet & Apkarian, 1994; Scherer et al., 1997), it can be seen that if the matrix inequalities

$$\mathscr{P} = \mathscr{P}^{\mathrm{T}} > 0, \tag{13}$$

$$\begin{pmatrix}\mathscr{A}_i^{\mathrm{T}}\mathscr{P} + \mathscr{P}\mathscr{A}_i & \mathscr{P}\mathscr{B}_i & \mathscr{C}_i^{\mathrm{T}}\\ \mathscr{B}_i^{\mathrm{T}}\mathscr{P} & -\gamma I & \mathscr{D}_i^{\mathrm{T}}\\ \mathscr{C}_i & \mathscr{D}_i & -\gamma I\end{pmatrix} < 0, \quad i \in \mathscr{I} \tag{14}$$

are feasible, GAS of the closed-loop PWL system (for $w = 0$) is indeed guaranteed and an $\mathscr{L}_2$ gain smaller than or equal to γ is obtained in the sense that for zero initial conditions, i.e. $\underline{x}_{CL}(0) = \underline{0}$ and all square integrable functions $w(t)$, the inequality

$$\|\,\underline{z}\,\|_2 \leqslant \gamma\|w\|_2 \tag{15}$$

holds with $\|\,\underline{z}\,\|_2^2 := \int_0^\infty \underline{z}(\tau)^{\mathrm{T}}\,\underline{z}(\tau)\,\mathrm{d}\tau$ and $\|w\|_2^2 := \int_0^\infty w(\tau)^{\mathrm{T}}w(\tau)\,\mathrm{d}\tau$. Here, $\underline{z}(t)$ denotes the response of the PWL closed-loop system (9) with input $w(t)$ and $\underline{x}_{CL}(0) = \underline{0}$. This means that the induced L_2-norm of the operator from w to $\underline{z}$ is smaller than γ under zero initial conditions for all nonzero $w \in L_2$.

Indeed, if (13) and (14) are satisfied for a controller as in (8) and a matrix $\mathscr{P}$, then it can be shown that the storage function $V(\underline{x}_{CL}) = \underline{x}_{CL}^{\mathrm{T}}\mathscr{P}\underline{x}_{CL}$ satisfies $\mathrm{d}V(\underline{x}_{CL})(t)/\mathrm{d}t \leqslant -\underline{z}^{\mathrm{T}}(t)\,\underline{z}(t) + \gamma w^2(t)$. By integration of this inequality and using that $V(0) = 0$, it can be shown that an $\mathscr{L}_2$ gain smaller than or equal to γ from $w(t)$ to $\underline{z}(t)$ is realized for the closed-loop PWL system with zero initial conditions. Interestingly, since the chosen weighting filters do not depend on the mode i of the system, the signal interpretation of the $\mathscr{L}_2$ gain including the filters, can be used for the PWL system. Moreover, the $\mathscr{L}_2$ gain of the PWL system forms an upperbound on the H_∞ norm for the individual linear subsystems. This result can be used to evaluate the PWL controller in the frequency domain, at least for each subsystem (cf. also the case study below).

[1] As in Johansson and Rantzer (1998) one could also use *continuous* piecewise quadratic Lyapunov functions of the form $V(\underline{x}_{CL}) = \underline{x}_{CL}^{\mathrm{T}}\mathscr{P}_i\underline{x}_{CL}$ when x_s lies in region $\mathscr{X}_i$. However, the form of the regions $\mathscr{X}_i$ would automatically lead to a common quadratic Lyapunov function, i.e. $\mathscr{P}_i = \mathscr{P}$, $i = 1, 2, 3$.

Eqs. (13) and (14) are nonlinear matrix inequalities in the variables $\mathscr{P}$, $A_{K,i}$, $B_{K,i}$, C_K, D_K and γ, $i \in \mathscr{I}$. By partitioning $\mathscr{P}$ and $\mathscr{P}^{-1}$ as

$$\mathscr{P} = \begin{pmatrix} Y & N \\ N^{\mathrm{T}} & * \end{pmatrix}, \quad \mathscr{P}^{-1} = \begin{pmatrix} X & M \\ M^{\mathrm{T}} & * \end{pmatrix}, \tag{16}$$

where X and Y are $n \times n$ symmetric matrices, with n the dimension of the state vector $\underline{x}(t)$ in (7), and by using the following linearizing change of variables given in Scherer et al. (1997)

$$\begin{aligned} \widehat{A}_i &= NA_{K,i}M^{\mathrm{T}} + NB_{K,i}CX \\ &\quad + YB_{u,i}C_KM^{\mathrm{T}} \\ &\quad + Y(A_i + B_{u,i}D_KC)X, \quad i \in \mathscr{I}, \\ \widehat{B}_i &= NB_{K,i} + YB_{u,i}D_K, \\ \widehat{C}_i &= C_KM^{\mathrm{T}} + D_KCX, \\ \widehat{D}_i &= D_K \end{aligned} \tag{17}$$

the matrix inequalities (13) and (14) can be reformulated as linear matrix inequalities (LMIs) with the free variables X, Y, $\widehat{A}_i$, $\widehat{B}_i$, $\widehat{C}$, $\widehat{D}$, and γ, $i \in \mathscr{I}$:

$$\begin{pmatrix} X & I \\ I & Y \end{pmatrix} > 0, \tag{18}$$

$$\begin{pmatrix} A_iX + XA_i^{\mathrm{T}} + B_{u,i}\widehat{C}_i + (B_{u,i}\widehat{C}_i)^{\mathrm{T}} & * & * & * \\ \widehat{A}_i + (A_i + B_{u,i}\widehat{D}_iC_i)^{\mathrm{T}} & A_i^{\mathrm{T}}Y + YA_i + \widehat{B}_iC_i + (\widehat{B}_iC_i)^{\mathrm{T}} & * & * \\ (B_{w,i} + B_{u,i}\widehat{D}_iD_{w,i})^{\mathrm{T}} & (YB_{w,i} + \widehat{B}_iD_{w,i})^{\mathrm{T}} & -\gamma I & * \\ C_{z,i}X + D_{zu,i}\widehat{C}_i & C_{z,i} + D_{zu,i}\widehat{D}_iC_i & D_{zw,i} + D_{zu,i}\widehat{D}_iD_{w,i} & -\gamma I \end{pmatrix} < 0, \quad i \in \mathscr{I}. \tag{19}$$

Since γ enters linearly in (19), it can be directly minimized by LMI optimization to find the smallest achievable $\mathscr{L}_2$ gain of the closed-loop system (9) that can be found by using a quadratic storage function. These LMIs can be solved efficiently using commercially available software (Gahinet, Nemirovski, Laub, & Chilali, 1994). After a feasible solution has been found, nonsingular matrices M and N can be calculated using a singular value decomposition and the identity $MN^{\mathrm{T}} = I - XY$, which follows from (16). Afterwards, the controller matrices can be calculated from (17). See Scherer et al. (1997) for more details.

3.2. Control design

Both the weighting filters for shaping the sensitivity function, W_e, and the filter for shaping the control sensitivity function, W_u, are chosen the same for each region, such that in each region these transfer functions are designed to have the same shape. The filters are designed to be both stable and biproper such that no unstable dynamics are inserted which cannot be stabilized by the controller (Skogestad & Postlethwaite, 2005). The filter W_e is used to enforce a desired bandwidth and an integral action in the high level sheet controllers. Since in each region the plant to be controlled consists of an integrator, a second order filter is needed to enforce the integral action:

$$W_e(s) = \frac{1}{S_0} \frac{\dfrac{1}{4\pi^2 f_{BW} f_I}s^2 + \left(\dfrac{0.7}{2\pi f_{BW}} + \dfrac{0.7}{2\pi f_I}\right)s + 1}{\dfrac{S_\infty}{4\pi^2 S_0 f_{BW} f_I}s^2 + \dfrac{2 \cdot 0.7\sqrt{S_\infty}}{2\pi\sqrt{S_0 f_{BW} f_I}}s + 1}. \tag{20}$$

Here, f_{BW} is used to tune the bandwidth and f_I represents the desired cut-off frequency of the integral action. Furthermore, S_0 represents the upper bound on the amplitude of the sensitivity function for $s \to 0$, whereas S_∞ represents the upper bound on the amplitude for $s \to \infty$. Here, f_{BW} and f_I have been chosen to be 12 Hz and 2.4 Hz, respectively, whereas the upper bounds have been chosen to be $S_0 = 10^{-150/20}$ and $S_\infty = 10^{6/20}$. In the low-frequency range W_e has a zero slope, to prevent inserting a pole in $\omega = 0$ in the augmented plant that cannot be stabilized by the controller. For mid-range frequencies W_e has a slope of -2, corresponding to the desired -1 slope of the controller, i.e. the integral action, and the -1 slope of the high level sheet dynamics. This can be seen in Fig. 7, which shows the inverse of W_e. For high frequencies, W_e again has a zero slope.

In Fig. 4, W_u is selected to represent a matrix with a SISO weighting filter w_u on each diagonal element and with zeros on all other elements. By weighting each control input with the weighting filter given by

$$w_u(s) = \frac{\dfrac{1}{2\pi f_{ro}}s + 1}{\dfrac{R_\infty}{2\pi f_{ro}}s + R_0}, \tag{21}$$

a high frequency roll-off can be enforced in the controller. In (21), f_{ro} represents the desired roll-off frequency, whereas R_0 and R_∞ represent the upper bound on the amplitude of the control sensitivity when $s \to 0$ and $s \to \infty$, respectively. The filter parameters are chosen to be $f_{ro} = 50$ Hz, $R_0 = 10^{100/20}$, and $R_\infty = 10^{40/20}$, resulting in the filter shown in Fig. 8. Since $S_i \approx 1$ for frequencies well above the bandwidth, the control sensitivity R_i can be approximated by the controller in this region. Hence, for high frequencies the controller is weighted and therefore the desired roll-off can be shaped.

Given the sheet dynamics (2), together with the weighting filters (20) and (21), a feasible solution of the

LMIs (18)–(19) can be found as mentioned in Section 3.1. The resulting value of γ is $\gamma = 0.58$.

The Bode plot of the controller for the first subsystem of the sheet dynamics can be seen in Fig. 5. From this figure it becomes clear that both the desired integral action and the high frequency roll-off have been realized. Using the controller and the sheet dynamics active in the first region of the PWL model, the loop gain for this region can be calculated, resulting in the Bode plot shown in Fig. 6. From this figure, it can be seen that the bandwidth of the first controlled subsystem is approximately 10 Hz, which is significantly lower than typical bandwidths of the low level motor control loops (in the order of 50 Hz), as required in an hierarchical control setup. From Fig. 6, also the stability of the first subsystem can be observed, as this is guaranteed by the design. Since at the crossover frequency the phase lag is approximately 110°, the subsystem is stable and the phase margin is approximately 70°.

As already remarked in Section 3.1, the found $\mathscr{L}_2$ gain of the PWL system is an upperbound on the H_∞ norm of the individual linear subsystems, and the frequency domain interpretation of the H_∞ norm can be used for evaluating the controllers in each regime. As such, consider in Fig. 7 the Bode plot of the designed sensitivity function of the first subsystem, together with the inverse of the weighting filter W_e. It can be seen that $|S_1(j\omega)| < |W_e^{-1}(j\omega)|, \forall\omega$, which leads to the conclusion that the obtained sensitivity function meets the design criteria. The same conclusion can be drawn for the control sensitivity function that has been designed. As can be seen from Fig. 8, which shows the inverse of the weighting filter w_u together with the control

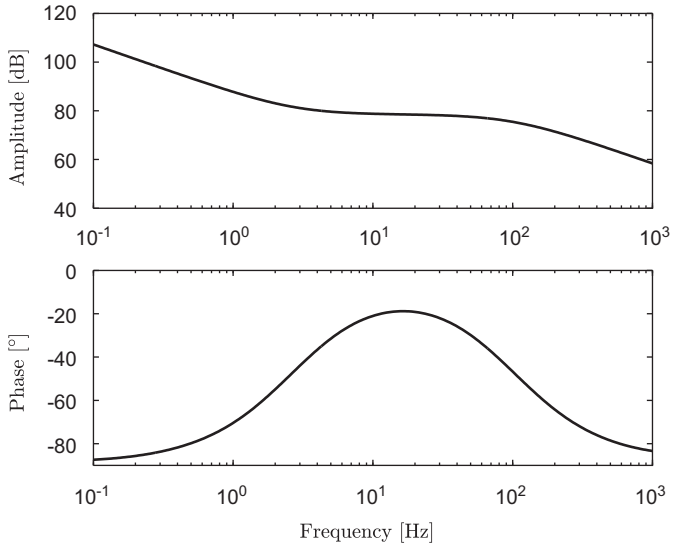

Fig. 5. Sheet feedback controller of the first subsystem.

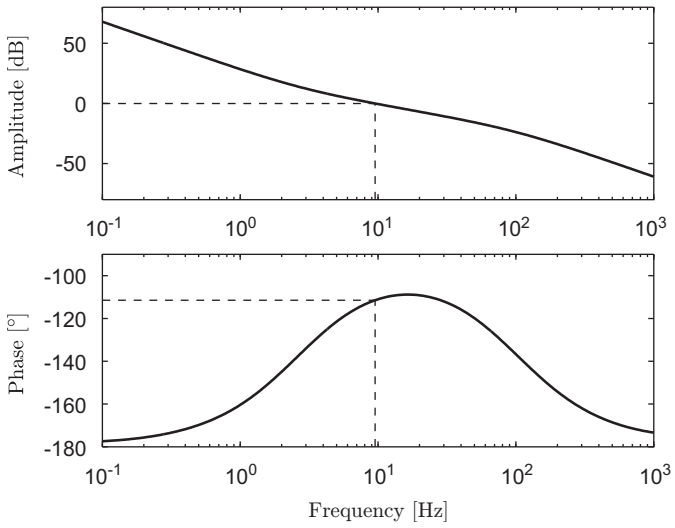

Fig. 6. Loop gain of the first subsystem.

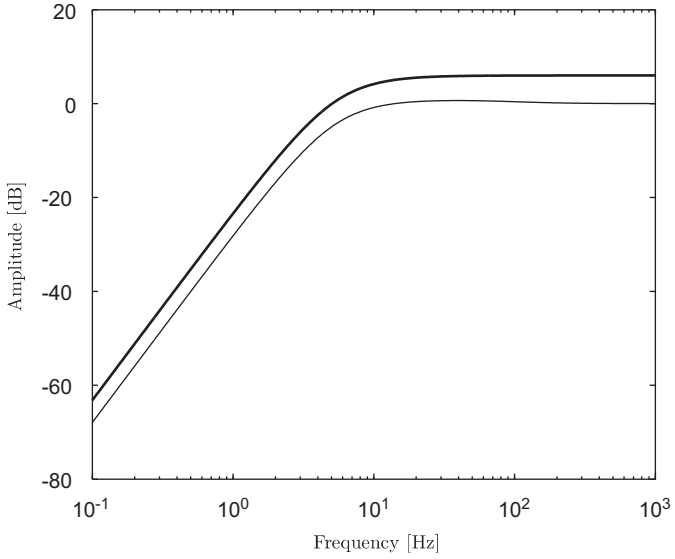

Fig. 7. W_e^{-1} (thick) and S_1 (thin).

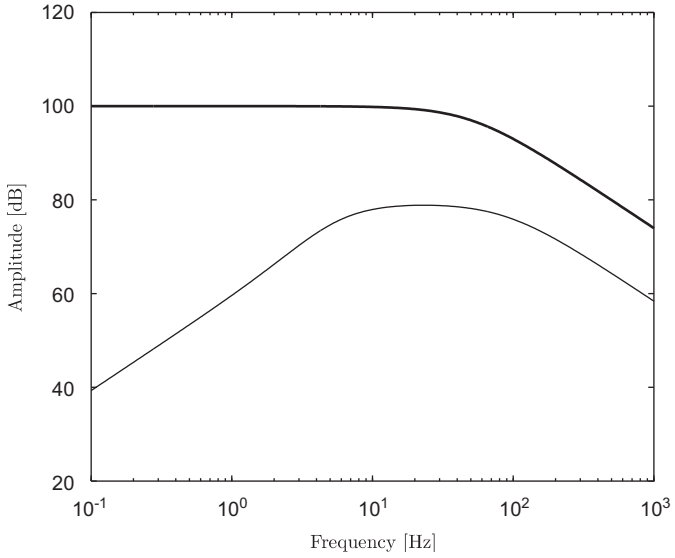

Fig. 8. w_u^{-1} (thick) and R_1 (thin).

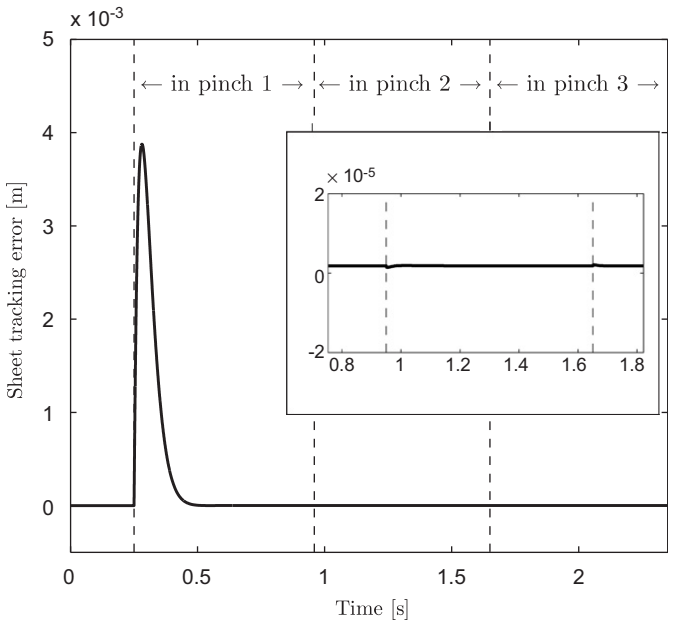

Fig. 9. Sheet tracking error obtained in simulation.

sensitivity function of the first subsystem, also in this case the inverse of the weighting filter upperbounds the corresponding closed-loop transfer function: $|R_1(j\omega)| < |w_u^{-1}(j\omega)|, \forall\omega$.

3.3. Simulation results

Simulations have been conducted for the basic paper path case-study in order to demonstrate the effectiveness of the control design approach. For the sheet motion task, a constant velocity of $0.3\,\mathrm{m\,s^{-1}}$ is chosen that has to be tracked throughout the paper path. The corresponding sheet position reference profile is therefore a ramp function. In the simulation, the parameters for the basic paper path are chosen equal to the nominal ones, given in Section 2. The resulting sheet tracking error obtained from simulation is depicted in Fig. 9. Since no feedforward controllers have been used, the pinches are standing still when the sheet arrives at the first pinch. Due to the difference between the reference velocity and the initial actual velocity the error starts increasing. However, the initial sheet tracking error quickly decreases towards zero.

4. Robust control design

Although the control design approach presented in the previous section inherently introduces robustness against model uncertainties up to a certain degree, no guarantees can be given as these uncertainties were not explicitly taken into account in the control design. Therefore, this section presents a control design approach that guarantees stability and performance of the system that is subject to model uncertainties.

4.1. Uncertainty modeling

The robust control design discussed in this section will be carried out based on the PWL high level sheet model with uncertain paper path parameters, e.g. tolerances on the pinch radii:

$$\dot{x}_s(t) = (B_i + \Delta B_i)\,\underline{u}(t), \quad x_s(t) \in \mathscr{X}_i,\ i \in \mathscr{I}. \tag{22}$$

The control goal in this section is to make the system robustly stable for the parameter uncertainties. Furthermore, robust performance has to be realized. Hence, performance conditions will have to be satisfied for all possible plants, i.e. including the worst-case uncertainty (Skogestad & Postlethwaite, 2005). To realize this goal, the H_∞ control paradigm presented in Section 3.1 is used and extended to include the uncertainties in the parameters into the design framework.

The first topic to be addressed in the robust control design approach is to determine the uncertainty set, i.e. to find a mathematical representation of the model uncertainty (Skogestad & Postlethwaite, 2005; Terlouw, Lambrechts, Bennani, & Steinbuch, 1992). From (22) it can be observed that the structure of the model is known, but some of the parameters are uncertain. As a result, the uncertainties are parametric and real-valued. These uncertainties are quantified by assuming that the parameter combinations $\psi_i = n_i R_i$ in the input matrices B_i are bounded within some region $[\underline{\psi}_i, \overline{\psi}_i]$. In other words, parameter sets of the form

$$\psi_i = \tilde{\psi}_i(1 + r_{\psi,i}\delta_i), \quad i \in \mathscr{I}, \tag{23}$$

can be formulated. In (23), $\tilde{\psi}_i \triangleq (\overline{\psi}_i + \underline{\psi}_i)/2$ represents the mean parameter value, $r_{\psi,i} = (\overline{\psi}_i - \underline{\psi}_i)/(\overline{\psi}_i + \underline{\psi}_i)$ represents the relative uncertainty, and δ_i is any real scalar satisfying $|\delta_i| \leqslant 1$. Since the perturbation δ is real-valued, the parametric uncertainty can be represented in the H_∞ framework (Skogestad & Postlethwaite, 2005). This can be illustrated by rewriting the model of the sheet dynamics in each region in transfer function format:

$$G_{\delta,i}(s) = \Psi_i G_{0,i}(s), \quad i \in \mathscr{I}, \tag{24}$$

with $G_{\delta,i}$ representing the set of possible plants, $G_{0,i}(s) = \frac{1}{s}$, and $\Psi_1 = [\psi_1\ 0\ 0]$, $\Psi_2 = [0\ \psi_2\ 0]$, and $\Psi_3 = [0\ 0\ \psi_3]$. Given this representation, the parametric, real-valued uncertainty can be rewritten as a multiplicative input uncertainty:

$$G_{\delta,i}(s) = \underbrace{\tilde{\Psi}_i G_{0,i}(s)}_{G_i(s)}(I + W_{\delta,i}\Delta), \quad i \in \mathscr{I}, \tag{25}$$

with $\tilde{\Psi}_i$ defined as $\tilde{\Psi}_1 = [\tilde{\psi}_1\ 0\ 0]$, $\tilde{\Psi}_2 = [0\ \tilde{\psi}_2\ 0]$, and $\tilde{\Psi}_3 = [0\ 0\ \tilde{\psi}_3]$. Furthermore, $G_i(s)$ represents the nominal plant, $W_{\delta,i}$ is the uncertainty matrix for region i containing the relative uncertainty $r_{\psi,i}$ on the ith diagonal element and zeros on all the other elements, and Δ is a diagonal matrix containing real-valued scalars δ_i, with $|\delta_i| \leqslant 1$. Hence, for Δ

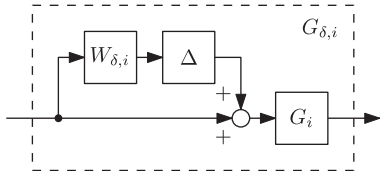

Fig. 10. Block scheme representing the multiplicative input uncertainty.

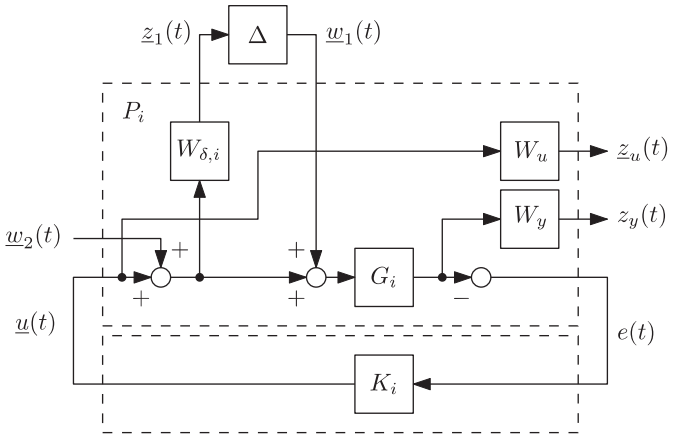

Fig. 11. Standard plant configuration for region i.

it holds that $\|\Delta\|_\infty \leqslant 1$. This multiplicative input uncertainty can be represented by the block diagram in Fig. 10.

4.2. Controller synthesis

With respect to the standard plant configuration used in Section 3.1 a few changes are made as can be seen in Fig. 11. First of all, the multiplicative input uncertainty has been included. Furthermore, the exogenous input $\underline{w}_2(t)$ now enters the loop before the plant instead of after, as was the case in Fig. 4. In this way it is ensured that the weighting filters W_u and W_y both weigh only one closed-loop transfer function. In the standard plant configuration shown in Fig. 11, the input and output resulting from the uncertainty are represented by $\underline{w}_1(t)$ and $\underline{z}_1(t)$, respectively. Furthermore, $\underline{z}_u(t)$ and $z_y(t)$, i.e. the weighted control input and the weighted plant output, represent the outputs to be minimized. As can be seen in Fig. 11 the weighting filter W_u can be used to shape the complementary sensitivity function

$$T_i = (I + G_i K_i)^{-1} G_i K_i, \quad i \in \mathscr{I}, \tag{26}$$

and can therefore be used to enforce a high frequency roll off in the controller. Furthermore, in combination with the filter W_y, it can be used to realize the desired bandwidth of the controlled system. On the other hand, the filter W_y is used for shaping the process sensitivity function and can therefore be used to enforce the integral action in the controller. Both filters can be represented in analogy with (4) and (6).

Given the standard plant configuration in Fig. 11, the robust controller synthesis procedure will be based on a common quadratic Lyapunov (storage) function, which aims at guaranteeing an $\mathscr{L}_2$ gain of the PWL closed-loop system smaller than or equal to $0 \leqslant \gamma < 1$ from $\underline{w} := [\underline{w}_1^{\mathrm{T}}\ \underline{w}_2^{\mathrm{T}}]^{\mathrm{T}}$ to $\underline{z} := [\underline{z}_1^{\mathrm{T}}\ z_y\ \underline{z}_u^{\mathrm{T}}]^{\mathrm{T}}$ for zero initial conditions. The construction of a robust controller of the form (8) and a corresponding quadratic storage function via LMIs that guarantees that the $\mathscr{L}_2$ gain is smaller than γ can be done in an identical manner as described in Section 3.1. If this construction is successful, it is indeed guaranteed that the induced $\mathscr{L}_2$-gain of the PWL closed-loop system from the performance input $\underline{w}_2$ to the performance output $[z_y\ \underline{z}_u^{\mathrm{T}}]^{\mathrm{T}}$ is smaller than $0 \leqslant \gamma < 1$ under zero initial conditions and for all plants in the uncertainty set $G_{\delta,i}$:

$$\left\| \begin{pmatrix} z_y \\ \underline{z}_u \end{pmatrix} \right\|_2 \leqslant \gamma \|\underline{w}_2\|_2. \tag{27}$$

This means that robust performance and robust stability are indeed warranted for the PWL closed-loop system (see Bukkems, 2007 for more details).

4.3. Control design

To study the robustness against uncertain system parameters, an additional transmission ratio of $\frac{16}{30}$ is chosen, as a result of which uncertainty in the transmission ratios is introduced. Given this transmission ratio together with the ones of Section 2, uncertainty matrices $W_{\delta,i}$ containing the relative uncertainties $r_{\psi,1} = 0.05$, $r_{\psi,2} = 0.07$, and $r_{\psi,3} = 0.03$, respectively, can be derived. As in Section 3.2 the filters W_y and w_u are again chosen the same for each region to enforce the same performance for each of the subsystems.

Since in each region the plant to be controlled consists of an integrator, whereas the desired sensitivity function has a $+2$ slope for low frequencies, the desired process sensitivity has a $+1$ slope in that frequency range. Therefore, W_y is chosen to be a first order filter:

$$W_y(s) = \frac{\frac{1}{2\pi f_I} s + 1}{\frac{S_{p,\infty}}{2\pi f_I} s + S_{p,0}}. \tag{28}$$

Here, f_I represents the desired cut-off frequency of the integral action, whereas $S_{p,0}$ and $S_{p,\infty}$ represent the upper bound on the amplitude of the process sensitivity function for $s \to 0$ and $s \to \infty$, respectively. After scaling the plant such that its gain equals 0 [dB] at the desired bandwidth, i.e. 10 Hz, f_I has been chosen to be 2 Hz, whereas the asymptotic amplitudes have been chosen to be $S_{p,0} = 10^{-60/20}$ and $S_{p,\infty} = 10^{12/20}$. The inverse of the resulting weighting filter W_y is shown in Fig. 14.

Since $T_i \approx K_i G_i$ for frequencies well above the bandwidth, the weighting filter w_u can be used to enforce a high frequency roll-off in the controller by shaping T_i. To realize this, a second order filter is needed, coinciding with

the -2 slope of K_iG_i at high frequencies:

$$W_u(s)=\frac{1}{T_\infty}\frac{\frac{1}{4\pi^2 f_{BW}f_{ro}}s^2+\left(\frac{0.7}{2\pi f_{BW}}+\frac{0.7}{2\pi f_{ro}}\right)s+1}{\frac{T_0}{4\pi^2 T_\infty f_{BW}f_{ro}}s^2+\frac{2\cdot 0.7\sqrt{T_0}}{2\pi\sqrt{T_\infty f_{BW}f_{ro}}}s+1}. \tag{29}$$

In (29), f_{BW} is used to tune the bandwidth and f_{ro} represents the desired roll-off frequency. Furthermore, T_0 represents the upper bound on the amplitude of the complementary sensitivity function for $s\to 0$, whereas T_∞ represents the upper bound on the amplitude for $s\to\infty$. The filter parameters values are chosen to be $f_{BW}=7$ Hz, $f_{ro}=50$ Hz, $T_0=10^{-120/20}$, and $T_\infty=10^{12/20}$. The inverse of the resulting filter W_u is shown in Fig. 15.

Based on the high level sheet dynamics, together with the designed weighting filters, a feasible solution of the LMIs (18)–(19) can be found, resulting in $\gamma=0.89$. Note that performance was traded in for robustness, as the obtained value of γ is larger than the one obtained in the nominal control design. Since the H_∞-norm of the Δ block shown in Fig. 11 is smaller than one and $\gamma<1$, the closed-loop system is stable, according to the small-gain theorem (Skogestad & Postlethwaite, 2005).

In Fig. 12, the Bode plot of the controller for the first subsystem of the sheet dynamics is shown. From the figure it becomes clear that both the desired integral action and the high frequency roll-off have been realized. Given the sheet feedback controller and the sheet dynamics active in the first region of the PWL model, the loop gain for this region can be calculated, resulting in the Bode plot shown in Fig. 13. From this figure, it can be seen that the bandwidth of the first controlled subsystem is approximately 10 Hz. Hence, also in this case the bandwidth is significantly lower than typical bandwidths of the low level motor control loops. From Fig. 13, the stability of the first subsystem can be observed, as this is guaranteed by the design. Since at the crossover frequency the phase lag is approximately 110°, the subsystem is stable and the phase margin is approximately 70°.

The Bode plot of the designed process sensitivity function of the first subsystem is shown in Fig. 14, together with the inverse of the weighting filter W_y. Since $|S_{p,1}(j\omega)|<|W_y^{-1}(j\omega)|$, $\forall\omega$, it can be concluded that the obtained process sensitivity function meets the design criteria. Since also $|T_1(j\omega)|<|w_u^{-1}(j\omega)|$, $\forall\omega$, the same conclusion can be drawn for the complementary sensitivity function, as can be seen in Fig. 15.

Given the controllers designed in this subsection, simulations have been carried out. The results of these simulations will be shown in Section 6.2.

5. Experimental setup

To validate the proposed control design, the experimental printer paper path setup depicted in Fig. 16 is used.

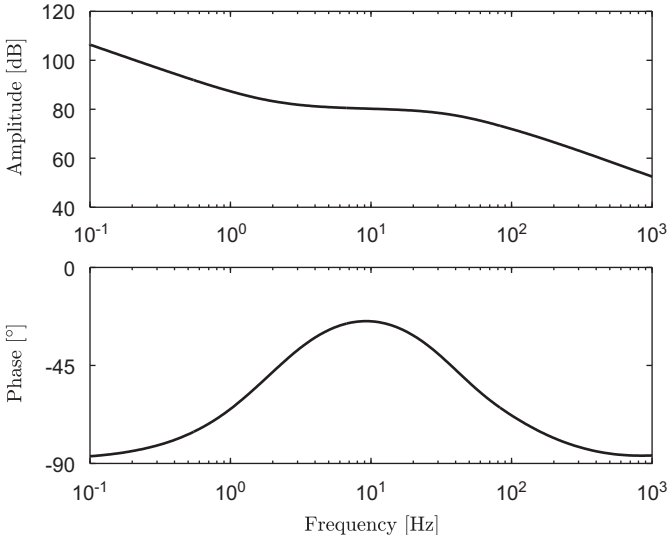

Fig. 12. Scaled sheet feedback controller of the first subsystem.

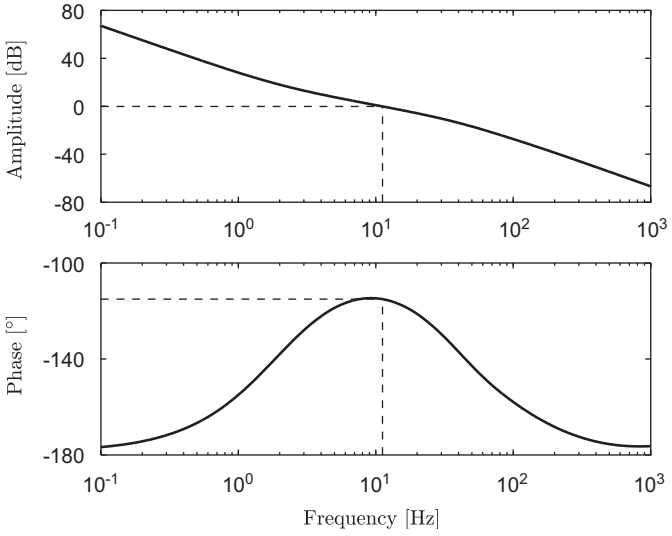

Fig. 13. Loop gain of the first subsystem.

It consists of a paper input module and a paper path with five pinches. In the experiments, the second, third and fourth pinch are the pinches where the actual control action takes place. In the remainder of this paper these pinches will be referred to as pinch 1, pinch 2, and pinch 3, respectively. Each pinch is connected to a motor via a gear belt. The transmission ratios are $n_1=\frac{18}{37}$, $n_2=\frac{16}{30}$ and $n_3=\frac{18}{37}$. Hence, they differ from the ones used in the control design but fall within the uncertainty regions. Consequently, the robustness of the closed-loop system can be studied. The radii of the pinches are 14×10^{-3} m. The angular position of the motors are measured via optical incremental encoders with a resolution of 2000 increments per revolution. The motors are 10 W DC motors driven by current amplifiers. Both the amplifiers and the encoders are connected to a PC-based control system. This system consists of three TUeDACS USB I/O devices (van de Molengraft, Steinbuch, & de Kraker, 2005), a Pentium 4

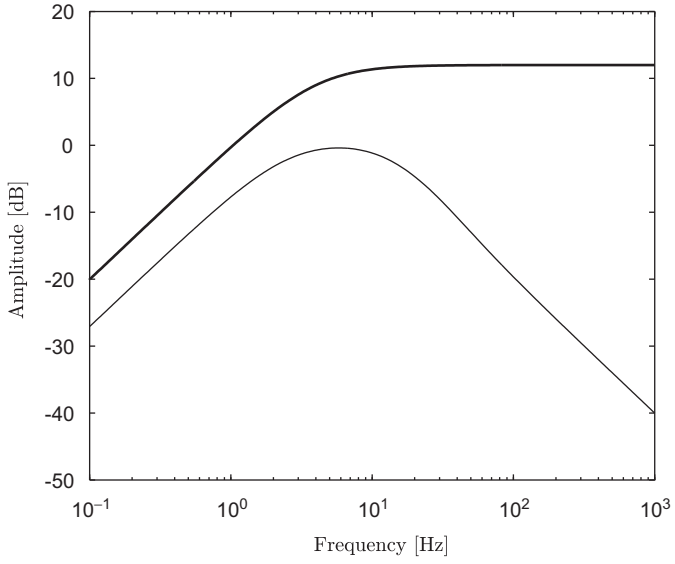

Fig. 14. W_y^{-1} (thick) and $S_{p,1}$ (thin).

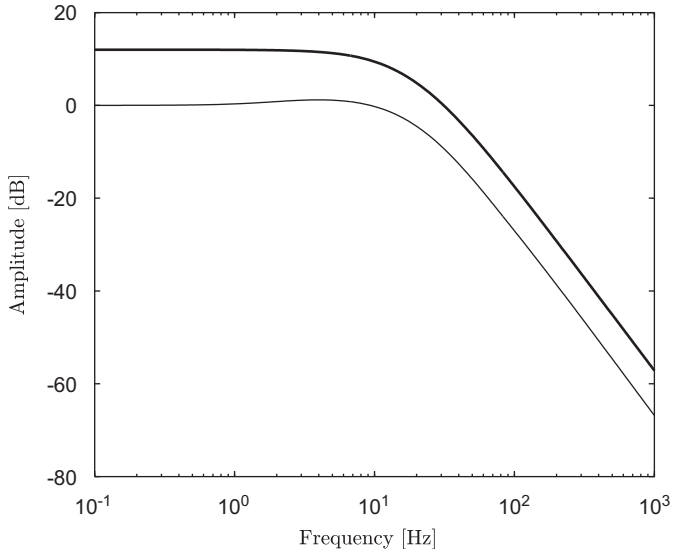

Fig. 15. $W_u(i,i)^{-1}$ (thick) and T_1 (thin).

host computer running RTAI/Fusion Linux and Matlab/Simulink/RTW. The sheets are guided through the paper path using thin steel wires and their position is measured using optical mouse sensors with a resolution of approximately 10 μm, which are directly connected to the host computer via USB. Both the high level and low level control loops are running in real-time at a fixed sampling rate of 1 kHz.

6. Experimental results

6.1. Low level motor control

In the design procedure of the sheet feedback controllers, perfect tracking behavior of the controlled motors has been assumed. Furthermore, infinitely stiff couplings between motors and pinches have been assumed. In a practical environment, however, these assumptions do not hold. Moreover, a digital implementation will cause delay in the loop which will limit the attainable bandwidth. Based on identified motor dynamics, PID feedback controllers have been designed using loopshaping techniques (Franklin et al., 1994). The controller parameters are tuned such that a bandwidth of 50 Hz is realized. The resulting closed-loop behavior is depicted in Fig. 17, which shows the frequency response function (FRF) of the complementary sensitivity of motor 1. Similar results are obtained for motors 2 and 3. From this figure it can be seen that the assumption on ideal low level motor dynamics is valid until approximately 10 Hz.

To investigate the stability of the overall system, i.e. the non-ideal low level motor control loops in combination with the high level sheet control loop, first the low level controlled motor dynamics have to be modeled. The delay, which is the bandwidth limiting factor for the low level motor control loops, should be taken into account in the models of the printer paper path. This can be done by using a pade approximation (Skogestad & Postlethwaite, 2005). On the other hand, the flexibilities due to the limited stiffness of the transmission belts can be neglected, since the resulting resonance manifests itself considerably above the bandwidth, see Fig. 17. Therefore the total low-level motor control loops consist of mass systems with delay controlled by PID controllers. Given the models of the low-level motor control loops, together with the high level sheet dynamics and the high level sheet feedback controllers calculated in Section 4.3, the model of the overall closed-loop system can be derived. The stability of this system can be analyzed using the LMIs (12)–(13), where $\mathscr{A}_i$ now represents the state matrix of the overall closed-loop system including the low level dynamics. Since a feasible solution of the LMIs can be found, the overall PWL closed-loop system is guaranteed to be stable.

6.2. Validation results

In the experimental validation of the control design, the focus is on studying the robustness of the system against parameter uncertainties. In this experiment the robust controllers calculated in Section 4.3 are used. The sheet reference motion task is to track a constant velocity of $0.3\,\mathrm{ms}^{-1}$ throughout the entire paper path. The sheet tracking errors obtained in the experiment and in simulation are given in Fig. 18. Since no feedforward control input has been used all pinches are standing still until a sheet enters the first pinch. The difference between the reference velocity and the initial actual velocity results in the large transient behavior just after the moment the sheet enters the paper path. However, this transient is quickly decreased by the sheet controller in the first regime. Furthermore, it can be noticed that the sheet tracking error increases when the sheet enters the second and third pinch. This is caused by the deviation of the implemented transmission ratios with respect to their nominal values.

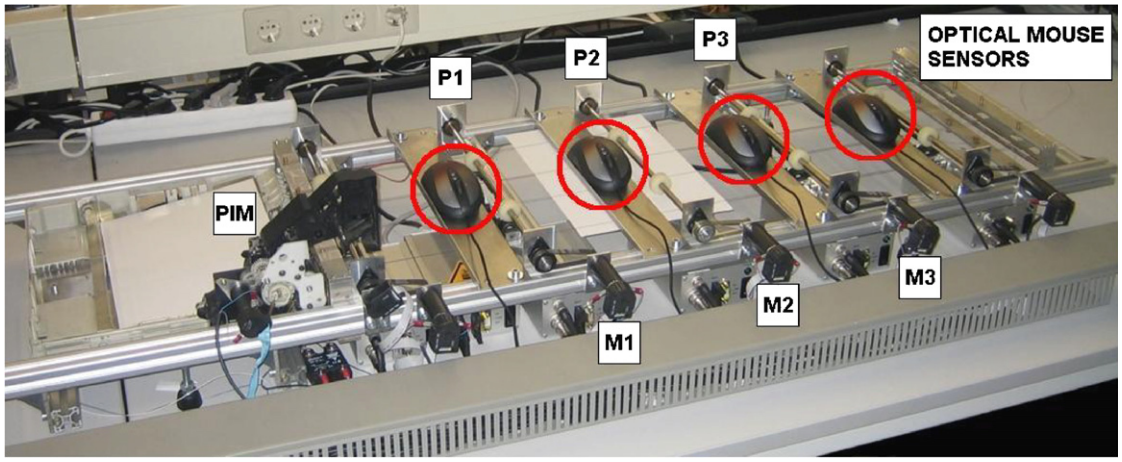

Fig. 16. The experimental printer paper path setup.

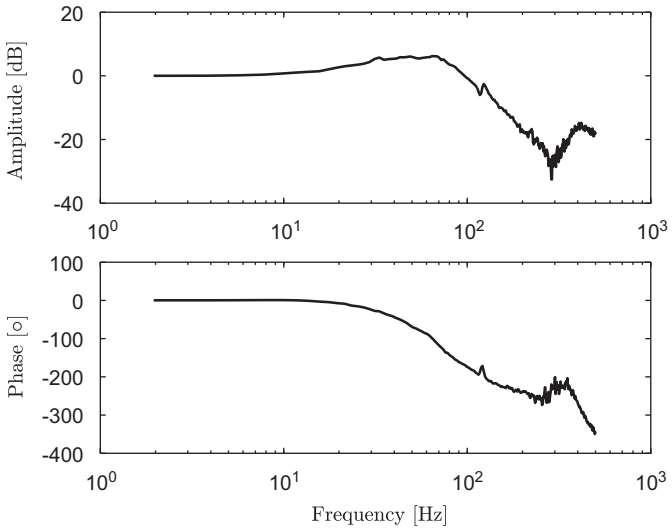

Fig. 17. FRF of the complementary sensitivity of motor 1.

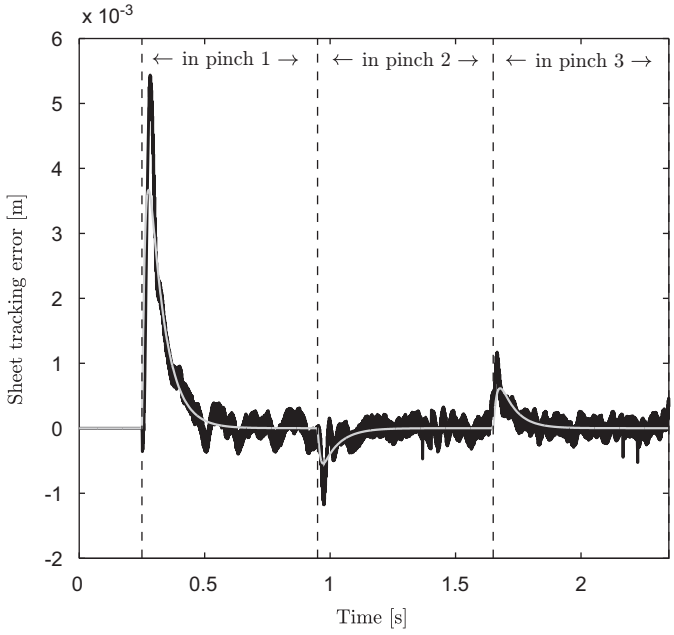

Fig. 18. Experimentally obtained tracking error (black) and the sheet tracking error obtained from simulation (gray).

Also these transient responses are controlled towards zero quickly. From Fig. 18, it appears that the closed-loop system is stable and robust for parameter uncertainties within the specified bounds. Furthermore, it can be seen that there is a close match between the experimental and simulation results. This close match justifies the assumption on ideal low level motor dynamics in the control design approach.

7. Conclusions and recommendations

In this paper, a control design approach for robust sheet feedback control in a printer paper path has been presented. Given a piecewise linear model of the sheet dynamics, piecewise linear output feedback controllers have been designed that guarantee robust stability and robust performance of the closed-loop PWL system. In the control design approach, linear H_∞ control design techniques have been combined with stability and performance requirements for the overall PWL system. To enable the practical implementation of the designed controllers on a test set-up of a printer paper path, cheap optical mouse sensors were used as sheet position sensors. Experimental results show that a stable closed-loop system has been obtained that is robust against system parameter changes within a specified bound. A major benefit of the introduction of (servo) feedback control in this application is that it provides the opportunity in industrial printers to use less expensive mechanics with larger tolerances, while still achieving the desired printing quality.

Future research will focus on releasing the simplifying assumptions for the basic paper path considered in this paper. More specifically, control design for cases in which multiple pinches are coupled into sections that are driven by one motor, and cases in which more than one pinch influence the sheet motion will be investigated. Some

relaxations have already been documented in Bukkems (2007). Secondly, since the handling of the sheet flow has improved as a consequence of the introduction of feedback control at the sheet level, the risk of sheets colliding in the paper path can be decreased. Hence, it is interesting to investigate the possibility of using less conservative sheet schedules, possibly resulting in a higher throughput of the system. Finally, it is of interest to continue the research line started in this paper to establish a further integration of the rich and powerful H_∞ frequency domain control design techniques for linear systems with the control design methods for hybrid systems.

References

Bukkems, B. (2007). *Sheet feedback control in a printer paper path*. Ph.D. thesis, Technische Universiteit Eindhoven, The Netherlands.

Bukkems, B., de Best, J., van de Molengraft, R., & Steinbuch, M. (2006). Robust piecewise linear sheet control in a printer paper path. *Second IFAC conference on analysis and design of hybrid systems* (*ADHS'06*), June 2006.

Chen, M., Zhu, C., & Feng, G. (2004). Linear-matrix-inequality-based approach to H1 controller synthesis of uncertain continuous-time piecewise linear systems. *IEE Proceedings—Control Theory Applications*, *151*(3), 295–300.

Cloet, C. (2001).*A mechatronics approach to copier paperpath design*. Ph.D. dissertation, University of California Berkely, CA, USA.

Feng, G. (2002a). Controller design and analysis of uncertain piecewise linear systems. *IEEE Transactions on Circuits and Systems I*, *49*(2), 224–232.

Feng, G. (2002b). An approach to H_∞ controller synthesis of piecewise linear systems. *Communications in Information and Systems*, *2*(3), 245–254.

Franklin, G., Powell, J., & Emami-Naeini, A. (1994). *Feedback control of dynamic systems* (3rd ed.). Reading, MA: Addison-Wesley Publishing Company.

Gahinet, P. (1996). Explicit controller formulas for lmi-based H_∞ synthesis. *Automatica*, *32*(7), 1007–1014.

Gahinet, P., & Apkarian, P. (1994). A linear matrix inequality approach to H_∞ control. *International Journal of Robust and Nonlinear Control*, *4*, 421–448.

Gahinet, P., Nemirovski, A., Laub, A., & Chilali, M. (1994). The LMI control toolbox. In *Proceedings of 1994 IEEE CDC* (Vol. 3, pp. 2038–2041).

Heemels, W., Schutter, B., & Bemporad, A. (2001). Equivalence of hybrid dynamical models. *Automatica*, *37*(7).

Johansson, M., & Rantzer, A. (1998). Computation of piecewise quadratic lyapunov functions for hybrid systems. *IEEE Transactions on Automatic Control*, *43*(4), 555–559.

Kruciński, M. (2000). *Feedback control of photocopying machinery*. Ph.D. dissertation, University of California Berkely, CA, USA.

van de Molengraft, R., Steinbuch, M., & de Kraker, M. (2005). Integrating experimentation into control courses. *IEEE Control Systems Magazine*, *25*(1), 40–44.

Rai, S. (1998). A hybrid hierarchical control architecture for paper transport systems. In *Proceedings of 1998 IEEE CDC* (Vol. 4, pp. 4294–4295).

Rantzer, A., & Johansson, M. (2000). Piecewise linear quadratic optimal control. *IEEE Transactions on Automatic Control*, *45*(4), 629–637.

Scherer, C., Gahinet, P., & Chilali, M. (1997). Multiobjective output-feedback control via LMI optimization. *IEEE Transactions on Automatic Control*, *42*(7), 896–911.

Skogestad, S., & Postlethwaite, I. (2005). *Multivariable feedback control analysis and design* (2nd ed). The Atrium, Southern Gate, Chichester, West Sussex PO19 8SQ, England: Wiley.

Sontag, E. (1981). Nonlinear regulation: The piecewise linear approach. *IEEE Transactions on Automatic Control*, *26*(2), 346–358.

Stephanopoulos, G. (1984). *Chemical process control*. Englewood Cliffs, NJ, USA: Prentice Hall.

Tang, Y., Landers, R., & Balakrishnan, S. (2006). Hierarchical optimal force-position-contour control of machining processes. *Control Engineering Practice*, *14*(8).

Terlouw, J., Lambrechts, P., Bennani, S., & Steinbuch, M., (1992). Parametric uncertainty modelling using lfts. *1992 AIAA guidance, navigation and control conference*, SC, USA.

Yasar, M., & Ray, A. (2007). Hierarchical control of aircraft propulsion systems: Discrete event supervisor approach. *Control Engineering Practice*, *15*(2), 149–192.

Zhou, K., Doyle, J., & Glover, K. (1996). *Robust and optimal control*. Upper Saddle River, New Jersey, USA: Prentice-Hall.